VIA MEDICA

ORIGINAL PAPER

Folia Histochem Cytobiol
Vol. 62, No. 4, 2024, pp. 180–190

DOI: 10.5603/fhc.101622
ISSN 0239-8508, e-ISSN 1897-5631

Opioid growth factor receptor overexpression exerts anti-hepatocellular carcinoma effects by activating P16 and P21 to inhibit proliferation and migration of HepG2 cells

Zhezhu Jin, Yongjun Jin

Department of Colorectal Surgery, Hangzhou Red Cross Hospital, Hangzhou, China

ABSTRACT

Introduction. Hepatocellular carcinoma (HCC) is the sixth most common type of cancer and the second leading cause of cancer death worldwide [19]. Opioid growth factor (OGF) has been shown to exhibit antitumour potential, binding to OGF receptor (OGFr). Naltrexone (NTX), an OGFr antagonist, is considered as a potential anti-cancer agent. However, the specific mechanism of how OGFr acts on HCC cells is yet to be elucidated.

Materials and methods. HepG2 cells were inoculated into subcutaneous areas of nude mice's back (200 μL, 2.5×10^7/mL) to establish HCC *in vivo* models. HepG2 cells were transfected with lentiviral plasmids containing short hairpin RNA (shRNA) targeting OGFr (sh-OGFr) or negative control shRNA (sh-NC), and OGFr over-expression (OE-OGFr) or over-expression negative control (OE-NC) plasmids. Subsequently, male BALB/c nude mice were randomized into Control, sh-NC, sh-OGFr, OE-NC, and OE-OGFr groups (n = 6). Tumour size was measured weekly for four weeks, TUNEL staining for apoptosis, and immunohistochemistry were performed. *In vitro*, HepG2 cells were randomized into OE-NC, OE-OGFr, and OE-OGFr+NTX (100 μmol/L) groups, and sh-NC, sh-OGFr, sh-OGFr+sh-P21, and sh-OGFr+sh-P16 groups. Cell viability by CCK8 assay, cell proliferation by EDU staining, cell migration by cell scratch, and Western blot were performed.

Results. *In vivo*, sh-OGFr-transfected HepG2 cells increased tumour weight, volume, and Ki67 expression, decreased P21 and P16 expression, and did not affect apoptosis rate. The effect of OE-OGFr in HepG2 cells was completely the opposite. *In vitro*, OE-OGFr inhibited HepG2 cells' viability, proliferation, and migration, and further NTX intervention reversed its inhibitory effects. The transfection of HepG2 cells with sh-OGFr+sh-P21 and sh-OGFr+sh-P16 further enhanced the cell proliferation and migration abilities compared to the sh-OGFr group.

Conclusions. OGFr overexpression may inhibit HCC progression by activating P16 and P21 expression to inhibit cell proliferation and migration, thereby providing new potential targets for HCC treatment.

Keywords: hepatocellular carcinoma; OGFr; cell proliferation; cell migration; P21; P16

Correspondence address:
Zhezhu Jin
Department of Colorectal Surgery,
Hangzhou Red Cross Hospital,
No. 208 East Huancheng Road,
Gongshu District,
Hangzhou 310003,
Zhejiang Province, China
e-mail: jinzhezhu_jzz2738@163.com

Submitted:
17 July, 2024
Accepted after reviews:
29 November, 2024
Available as Online first:
16 December, 2024

INTRODUCTION

As a primary malignant tumour of liver cells, hepatocellular carcinoma (HCC) represents the most common form of liver cancer, accounting for up to 90% of cases [1]. Men have a greater risk of developing liver cancer, with a global male-to-female incidence ratio of 2.8:1 [2]. The incidence of liver cancer is predicted to exceed 1 million cases by 2025 [1]. The onset of HCC remains insidious, with fewer than 30% of HCC patients being suitable for radical treatment at first diagnosis [3]. The survival rate of advanced

liver cancer patients receiving systemic treatment remains very poor [3, 4]. Furthermore, new biological therapies and small-molecule-targeted drug therapy remain imperfect and expensive, increasing the economic burden and pressure on quality of life, and thus have not been widely applied in clinical practice [4, 5]. Therefore, there is an urgent need for the emergence of effective, affordable, minimally toxic and safe therapies and the exploration of relevant targets for HCC treatment.

Opioid growth factor (OGF) is an endogenous pentapeptide, formerly known as methionine encephalin (MENK), acting in an autocrine and paracrine manner in several cancer cells such as ovarian and pancreatic cancer cells. It is not cytotoxic nor apoptosis-related, and exerts anti-tumour, anti-proliferative, anti-angiogenic, and cell renewal properties [6, 7]. OGF binds to its receptor (OGFr) to inhibit DNA synthesis, cell proliferation and cell growth, thereby modulating tumourigenesis and cancer progression [8]. Importantly, OGFr has been found to have no effects on cell necrosis or apoptosis [6]. Both *in vitro* and *in vivo* studies have reported that OGF leads to the inhibition of cell proliferation in human colon tumours, head and neck squamous cell carcinomas, and renal, ovarian and pancreatic cancers [9]. McLaughlin *et al.* [10] demonstrated that OGFr overexpression led to 11% to 68% decreases in cell number and 46% to 75% decreases in DNA synthesis in human squamous carcinoma cells of the head and neck, decelerating tumour growth. MENK has been shown to facilitate osteosarcoma cell proliferation, invasion and migration, which is reversed by further OGFr knockdown [11]. Moreover, OGFr expression has been observed in human HCC cells, with OGF inhibiting HCC cell proliferation and migration in mice, and exerting anti-HCC activity [12]. Avella *et al.* [13] noted the presence of OGFr in a human HCC cell line and verified its inhibitory effect on cell proliferation, and that the OGF-OGFr action was associated with DNA synthesis inhibition, independent of apoptosis or necrosis. However, the specific mechanism of OGF-OGFr axis in HCC remains to be identified.

It has been demonstrated that OGF-OGFr targets P21 and P16 by cyclin-dependent inhibitory kinase pathways to block the transition from G1 phase to S phase, inhibiting intracellular DNA synthesis and achieving effects for inhibition of normal cell proliferation [14]. Sikong *et al.* [12] demonstrated that OGFr knockdown led to decreased P21 and P53 expression in HCC cells, so as to inhibit cell proliferation and migration. It has been demonstrated *in vivo*, following cisplatin with OGF or cisplatin alone administered to HCC model mice respectively, that the combination group showed higher OGFr, P16, P21 and P53 levels than the cisplatin intervention group [12]. Furthermore, OGF-OGFr has been found to cause inhibition of head and neck squamous cell carcinoma cell proliferation by promoting the P16 pathway [15].

Therefore, we aimed to investigate the role and possible mechanism of the OGF-OGFr axis in HCC by constructing an HCC nude mouse subcutaneous graft tumour model and *in vitro* experiments to develop potential targets and new therapeutic strategies for clinical application of HCC therapy.

MATERIALS AND METHODS

Cell culture

Human hepatocellular carcinoma HepG2 cells (iCell-h092, iCell, Shanghai, China) were cultured in MEM (iCell-0012, iCell) with 10% foetal bovine serum (FBS; FS301-02, TransGene Biotech, Beijing, China) and 1% penicillin/streptomycin (FG101-01, TransGene) in a humidified cell culture incubator (BB150, Thermo Scientific, Waltham, MA, USA) under 5% CO_2, at 37°C, and 70–80% humidity. Observation of HepG2 cells morphology was done using a light microscopy (AE2000, Motic, Fujian, China).

Human normal hepatocytes (MIHA) cells (iCell-h054, iCell) and human HCC cell lines, including HepG2, Huh7 (iCell-h080, iCell), Hep3B (iCell-h091, iCell) and SK-Hep1 (iCell-h190, iCell) cells were cultured in DMEM with 10% FBS, 100 IU/mL penicillin and 100 μg/mL streptomycin under 5% CO_2 and at 37°C.

Cell transfection

OGFr knockdown, OGFr overexpression, P21 knockdown, and P16 knockdown cell lines were constructed using the lentiviral vector, LV3(H1/GFP&Puro). Sequence information was set out in Table 1. A collection of logarithmic growth phase HepG2 cells was made for transfection using a Lipofectamine™3000 kit (L3000-008, Invitrogen, Carlsbad, CA, USA) according to the manufacturer's instructions. HepG2 cells were infected with lentiviral plasmids containing short hairpin RNA (shRNA) targeting

Table 1. Sequences for transfection

Gene	Sequence
OGFR-homo-479	5′-AGGGAGGTCGAGGTGTTTAAA-3′
OGFR-homo-1246	5′-GGAGAAGATCGCTCTGAATTT-3′
OGFR-homo-243	5′-GTAGGTATCGGCACAACTATC-3′
P21-homo-533	5′-CAGATTTCTACCACTCCAAAC-3′
P21-homo-230	5′-AGCGATGGAACTTCGACTTTG-3′
P21-homo-419	5′-ATGTGGACCTGTCACTGTCTT-3′
P16-homo-142	5′-CCCAACGCACCGAATAGTTAC-3′
P16-homo-45	5′-GGGGAGCAGCATGGAGCCTTC-3′
P16-homo-267	5′-CCGACCCGTGCACGACGCTGC-3′

OGFr (sh-OGFr) or negative control shRNA (sh-NC), and OGFr over-expression (OE-OGFr) plasmid or over-expression negative control (OE-NC) plasmid. Following incubation for 8 h in an incubator at 37°C, and 5% CO_2, the medium was replaced with fresh complete medium to continue the incubation for 48 h. The transfection efficiency was detected by qRT-PCR assay.

Animals

6–8 week old healthy male BALB/c athymic nude mice, purchased from Shanghai Jihui Laboratory Animal Care Co., Ltd under NO.SCXK (Hu) 2022-0009, were housed in Hangzhou Huante Youjian Biotechnology Co., Ltd with NO.SYXK (Zhe) 2024-0003 following the guidelines of the Institutional Animal Care and Use Committee (approval number: ZJEY-20240215-01). The housing environment maintained a constant temperature of 22–24°C, 40–60% relative humidity, and a 12-hour light/dark cycle. Thenude mice were permitted free access to food and water for a week of acclimatisation, as well as subsequently.

Construction of xenograft tumour models and grouping

Following collection of HepG2 cells in logarithmic growth phase, adjustment of cell concentration to 2.5×10^7/mL was performed for inoculation into a subcutaneous area of the backs of the nude mice (200 μL) [16]. The status of the nude mice and transplanted tumour growth were observed weekly after inoculation. During this period, the mice were still kept in the SPF feeding room and fed *ad libitum*. Following pharmacological intervention and observation for four weeks, the nude mice were euthanised by inhalation of CO_2. The tumuor tissues was separated into two parts, one of which was fixed in 4% paraformaldehyde and sectioning after paraffin embedding, while the other part was frozen in liquid nitrogen and kept at –80°C.

Once the transplanted tumour volume reached 150 mm^3, the mice were randomly divided into five groups (n = 6 *per* group): Control, sh-NC, sh-OGFr, OE-NC, and OE-OGFr groups. The mice in the Control group received an equal amount of untransfected HepG2 cells.

Tumour weight and volume detection

The measurement of tumour size was carried out weekly from the modelling day, with calculation of the tumour volume and weight. The fascia was removed, and the tumours were cut out to record the tumour weight, with determination of long and short tumour diameters (a) and (b) using Vernier calipers. Tumour volume = $ab^2/2$ [17]. Tumour inhibition rate (%) = (1 — tumour volume of experimental group/tumour volume of Control group) × 100%.

Immunohistochemistry

Following dewaxing of tumour tissue paraffin sections, samples were gradually hydrated in decreasing ethanol gradients, washed with water, and incubated with 100 μL of 3% hydrogen peroxide blocking solution for 10 minutes at room temperature. The sections were placed in boiling antigen repair solution of 1 mmol Tris-EDTA (pH = 9.0, 648310, E9884, Sigma, St. Louis, MO, USA) for 15 minutes, held for 15 minutes, and then cooled naturally. The completion of thermal antigen repair and addition of 100 μL 5% BSA blocking solution was done at room temperature for 20 minutes. Subsequently, sections were reacted with primary antibodies, OGFr polyclonal antibody (1:200, PA5-77121, Invitrogen), Ki67 polyclonal antibody (1:200, AF0198, Affinity, OH, USA), P21 monoclonal antibody (1:1,000, ab188224, Abcam, Shanghai, China), and P16 monoclonal antibody (1:30, 270058, Abcam) overnight at 4°C. Incubation was performed with a secondary antibody, Goat-Anti-Rabbit H&L (HRP) (1:5,000, ab97080, Abcam), for 30 minutes at 37°C. DAB was added to develop colour, with haematoxylin (Bry-0001-01, Runnerbio, Shanghai, China) for re-staining for 30 s. Following rinsing in tap water, sections were sequentially put in graded ethanol and xylene, sealed, and observed under an E100 light microscope (Nikon, Tokyo, Japan). The appearance of yellow or brown colour (darker up to brown) in the cytoplasm was considered as a positive expression. The integral optical density (IOD) value and area value (sample area at 200× field of view) were analysed for each section (n = 6 *per* group), and the average optical density (AOD) was calculated using IOD/area value as a semi-quantitative analysis index.

TUNEL staining

The tumour tissue paraffin sections were stained with TUNEL followed the steps described in the TUNEL apoptosis detection kit (C1090, Beyotime, Shanghai, China) and incubated with DAPI staining solution (ab104139, Abcam) for 10 minutes at room temperature away from light, sealed, and examined microscopically. The nuclei of positive apoptotic cells were coloured in red. The numbers of positive cells (red) and total cells (blue) in each sample were measured by an Image J system, to calculate the number of positive cells/total cells as a positive cell rate.

CCK8 assay

The HepG2 cells were inoculated in 96-well plates for 48 h, and then the operation was completed according to the steps of a CCK8 kit (C0039, Beyotime). The OD values were measured at 0 h, 24 h, 48 h and 72 h to calculate the cell viability. Cell viability = (OD value of experimental group-blank zeroing OD value)/(OD value of control group-blank zeroing OD value) × 100%.

Cell grouping

The HepG2 cells were randomly divided into three groups for detection of the role of OGFr on HCC cell proliferation, including OE-NC, OE-OGFr, and OE-OGFr+naltrexone [18] (OGFr antagonist, NTX, 100 μmol/L, HY-17417A, MCE, Monmouth Junction, NJ, USA) groups. Meanwhile, the HepG2 cells were randomly divided into four groups, the sh-NC, sh-OGFr, sh-OGFr+sh-P21, and sh-OGFr+sh-P16 groups, to test the effects of P21 and P16 in OGFr regulation of HCC cell proliferation. Follow-up testing was accomplished after 48 h of incubation.

qRT-PCR

An RNA extraction kit (AG21024, Agbio, Hunan, China) was applied to obtain total RNA of HepG2 cells, and a HiFiScript cDNA synthesis kit (CW2569M, KangWei Co. Ltd., Beijing, China) was used to synthesise cDNA. Subsequently, qRT-PCR was accomplished by a SYBR Green qPCR kit (11201ES03, YiSheng Biotechnology Co. Ltd., Shanghai, China). The reaction conditions were as follows: 95°C, 10 min; 95°C, 15 s; 60°C, 60 s; 40 cycles. Glyceraldehyde-3-phosphate dehydrogenase (GAPDH) was taken as an internal reference gene. The relative OGFr, P21, and P16 mRNA expression were quantified by the $2^{-\Delta\Delta CT}$ assay. The primer sequences are set out in Table 2.

Cell scratch assay

A marker was used to draw five horizontal lines evenly behind a 6-well plate with an interval of 0.5 cm. 5×10^5 cells *per* well were cultured until the plate wells were spread and a straight line was drawn with the tip of a pipette gun. Cells under the scratches were washed away, and serum-free medium was added. Groups were treated for 24 h to observe the healing of scratches, and photographed. The scratch migration rate of cells in each group was analysed by Image J software. Cell migration rate = (0 h scratch width-scratch width after 24 h incubation)/0 h scratch width × 100%.

EDU test for cell proliferation

The culture of HepG2 cells was carried out in 12-well plates at a density of 60–70% and incubated with 500 μL of 2×EDU solution from a Beyoclick™ Edu-594 Cell Proliferation Detection Kit with Alexa Fluor 594 (C0078S, Beyotime) *per* well for 4 h at 37°C. Following fixation with 95% ethanol for 15 minutes at room temperature and permeabilisation with 0.3% TritonX-100 for 10 minutes, the samples were incubated with 0.5 mL of Click reaction solution for 30 minutes at room temperature. 1 mL of 1 × Hoechst 33342 solution from a Beyoclick™ Edu-594 Cell Proliferation Detection Kit was added to each well, and incubated for 2 minutes avoiding light. The slices were sealed and photographed under an inverted fluorescence microscope (Ts2-FC, Nikon). The number of cells and EDU-stained positive cells were measured by the Image J system, and the positive rate of each sample was counted as a quantitative analysis index. Positive rate = number of positive cells/total number of cells × 100%.

Western blot

The RIPA lysis buffer (P0013B, Beyotime) was used for lysis of HepG2 cells, and a BCA kit (pc0020, Beyotime) was used to detect the total protein concentration (0.30 mg/mL). The transfer of separated obtained proteins to PVDF membrane (10600023, GE Healthcare Life, Chicago, IL, USA) was accomplished using SDS-PAGE. Following 5% skimmed milk powder blocking, the incubation of protein samples with primary antibody (Table 3) overnight at 4°C and then with secondary antibody (Table 3) for 1 h was carried out. An ECL chemiluminescence meter (610020-9Q, Clinx, Shanghai, China) was applied for the measurement of protein bands.

Statistical analysis

Statistical data analysis was performed by SPSS software (version 20.0, IBM). Measurements between multiple groups that met normal distribution and chi-square were carried out by one-way analysis of variance (ANOVA). Further two--by-two comparisons were performed using the Tukey test. All statistics were reported as mean ± standard deviation. A P value of less than 0.05 was considered statistically significant.

Table 2. Primer sequences

Gene	Sequence
Human OGFr	Forward primer: 5′-GAGGACGAGGAGTCGGAGG-3′ Reverse primer: 5′-TGGCAGAAGACTCCACCTCT-3′
Human P21	Forward primer: 5′-CAGAACCGGCTGGGGATGT-3′ Reverse primer: 5′-GGAGTGGTAGAAATCTGTCATGC-3′
Human P16	Forward primer: 5′-CCGAATAGTTACGGTCGGAGG-3′ Reverse primer: 5′-AATCGGGGATGTCTGAGGGA-3′
Human β-actin	Forward primer: 5′-GCACCGTCAAGGCTGAGAAC-3′ Reverse primer: 5′-TGGTGAAGACGCCAGTGGA-3′

Table 3. Antibody information

Antibody	Company	Article number	Dilution
P21 antibody	Affinity	AF6290	1:1,000
P16 antibody	CST	18769S	1:1,000
P53 antibody	Affinity	AF0879	1:1,000
Anti-rabbit IgG, HRP-linked antibody	CST	7074	1:6,000
GAPDH antibody	Proteintech	10494-1-AP	1:10,000

Abbreviations: CST — Cell Signalling Technology; GAPDG — glyceraldehyde--3-phosphate dehydrogenase.

RESULTS

OGFr overexpression intervention led to tumour growth inhibition in HCC mice

HepG2 cell morphology was observed by light microscopy (Fig. 1A). HepG2 cells exhibited adherent growth, spindle-shaped or irregular polygonal cell morphology, clear cell edges, and clustered growth. The transfection efficiency of OGFr knockdown and overexpression in HepG2 cells was detected by qRT-PCR assay (Fig. 1B). The sh-OGFr group had lower OGFr mRNA levels than the sh-NC group ($P < 0.01$). Increased OGFr mRNA expression occurred in HepG2 cells of the OE-OGFr group compared

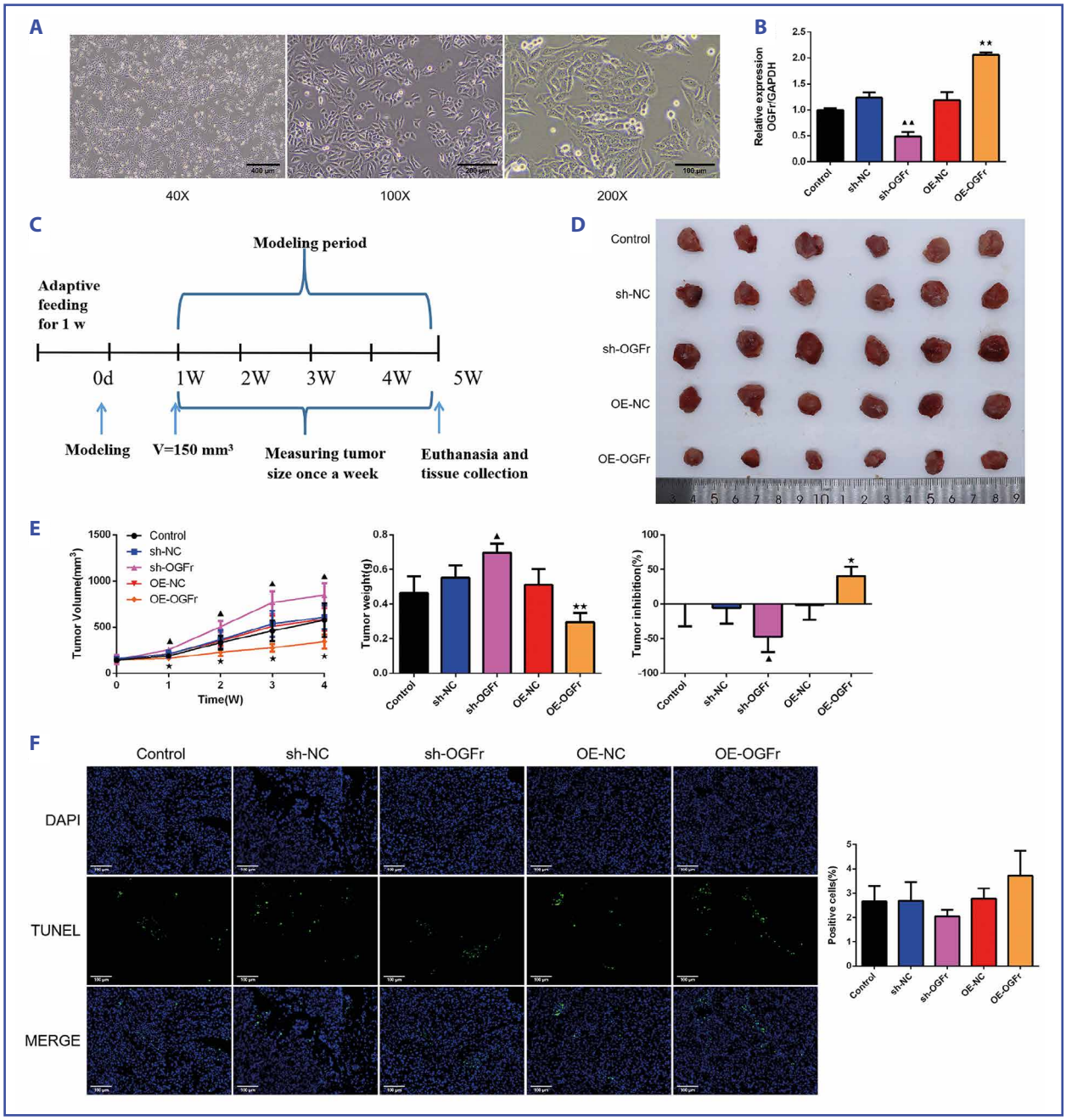

Figure 1. OGFr overexpression intervention led to tumour growth inhibition in HCC mice; **A.** Morphology of cultured HepG2 cells; **B.** Transfection efficiency of OGFr knockdown and overexpression in HepG2 cells was assessed by qRT-PCR, n = 3, ▲P < 0.05 and ▲▲P < 0.01 *vs.* sh-NC group, ★P < 0.05 and ★★P < 0.01 *vs.* OE-NC group; **C.** Flowchart of animal model of HCC in which male BALB/c nude mice received control or transfected HepG2 cells; **D.** Tumour size of mice four weeks after inoculation of transfected HepG2 cells, n = 6; **E.** Tumour volume and tumour weight at 1, 2, 3, and 4 weeks after inoculation of transfected HepG2 cells from cells' administration; tumour inhibition rate was calculated as described in 'Materials and methods', n = 6 for each group; **F.** Apoptosis of mouse tumour tissues was detected by TUNEL staining four weeks after inoculation of transfected HepG2 cells (magnification: 200×, scale bar: 100 μm), n = 6. ▲P < 0.05 and ▲▲P < 0.01 *vs.* sh-NC group, ★P < 0.05 and ★★P < 0.01 *vs.* OE-NC group. Abbreviations: HCC — hepatocellular carcinoma; OGFr — opioid growth factor receptor; qRT-PCR — quantitative reverse transcription polymerase chain reaction

to those of the OE-NC group ($P < 0.01$). The experiment flowchart was concisely diagrammed as displayed in Fig. 1C. The tumour weight and tumour volume at weeks 1, 2, 3, and 4 in the sh-OGFr group were higher ($P < 0.05$), with a decreased tumour inhibition rate compared to that of the sh-NC group (Fig. 1D, E, Suppl. Tab. S1–S3, $P < 0.05$). The OE-OGFr group had reduced tumour weight and tumour volume calculated at weeks 1, 2, 3, and 4 ($P < 0.01$ or $P < 0.05$), whereas there was an enhanced tumour inhibition rate compared to the OE-NC group (Fig. 1D, E; $P < 0.05$). Moreover, apoptosis of mouse tumour tissues in various groups was measured using TUNEL staining (Fig. 1F). The OE-OGFr group presented an elevated trend of apoptosis with respect to the OE-NC group, whereas a decreasing trend of apoptosis occurred in the sh-OGFr group compared to the sh-NC group ($P > 0.05$).

OGFr overexpression intervention caused elevated P21 and P16 expression and decreased Ki67 expression in HCC mice

OGFr, Ki67, P21, and P16 expression was measured using immunohistochemistry (Fig. 2). There were higher Ki67 expression ($P < 0.01$), and reduced OGFr, P21, and P16 expression ($P < 0.01$) in tumour tissues of sh-OGFr group compared to the sh-NC group. The Ki67 expression in the OE-OGFr group was lower than that of the OE-NC group, with enhanced OGFr, P21, and P16 expression ($P < 0.01$).

OGFr overexpression inhibited HepG2 cell viability, cell proliferation and migration

Detection of OGFr expression in MIHA, HepG2, Huh7, Hep3B, and SK-Hep1 cells was made by qRT-PCR assay (Fig. 3A). We intuitively visualized that increased OGFr mRNA

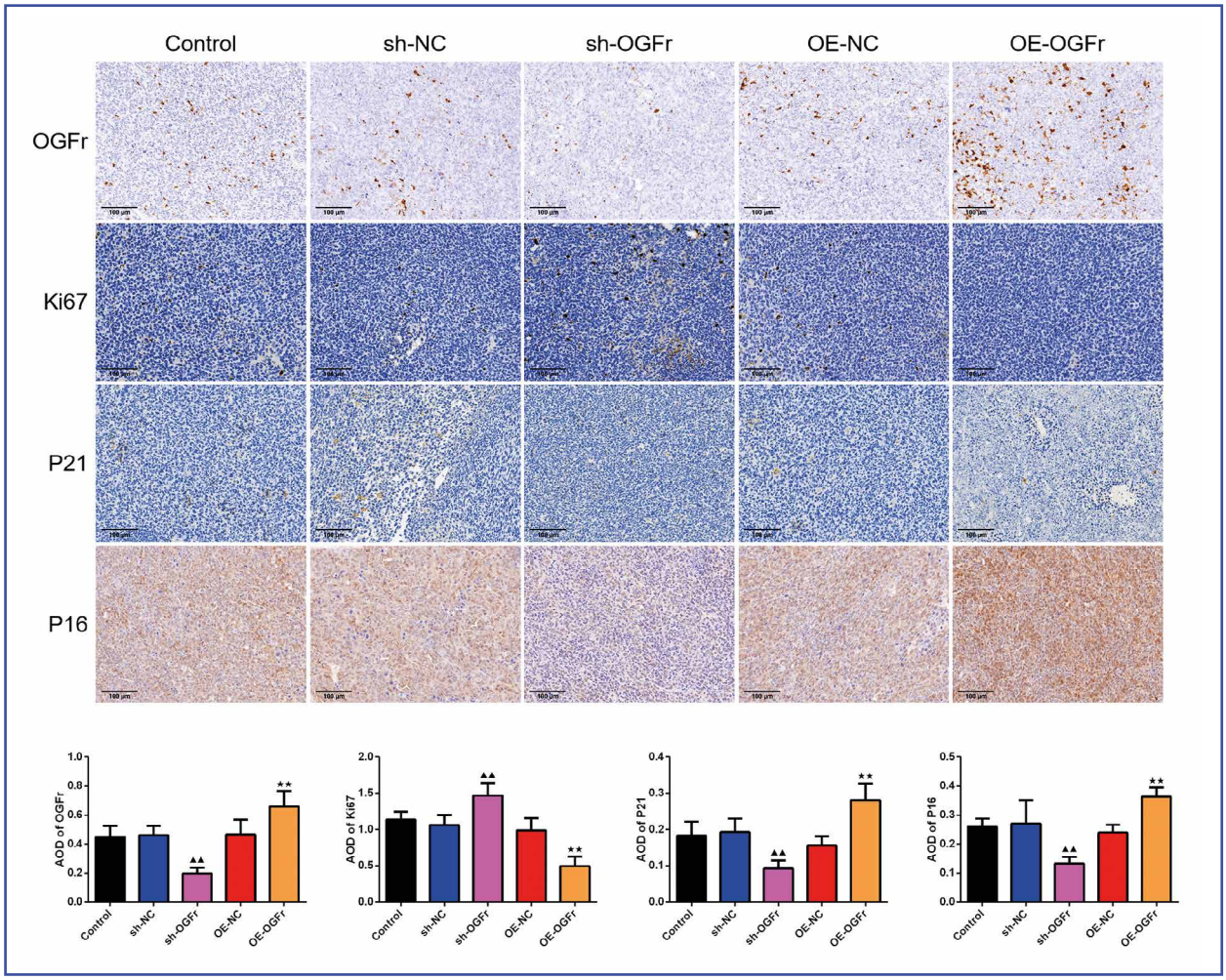

Figure 2. OGFr overexpression caused elevated P21 and P16 expression and decreased Ki67 expression in HCC mice. OGFr, Ki67, P21, and P16 expression was measured using immunohistochemistry (magnification: 200×, scale bar: 100 μm), n = 6; OGFr overexpression elevated P21 and P16 immunoreactivity and decreased Ki67 expression in HCC tumours in mice. ▲$P < 0.05$ and ▲▲$P < 0.01$ *vs.* sh-NC group, ★$P < 0.05$ and ★★$P < 0.01$ *vs.* OE-NC group. Abbreviations: AOD — average optical density; OGFr — opioid growth factor receptor

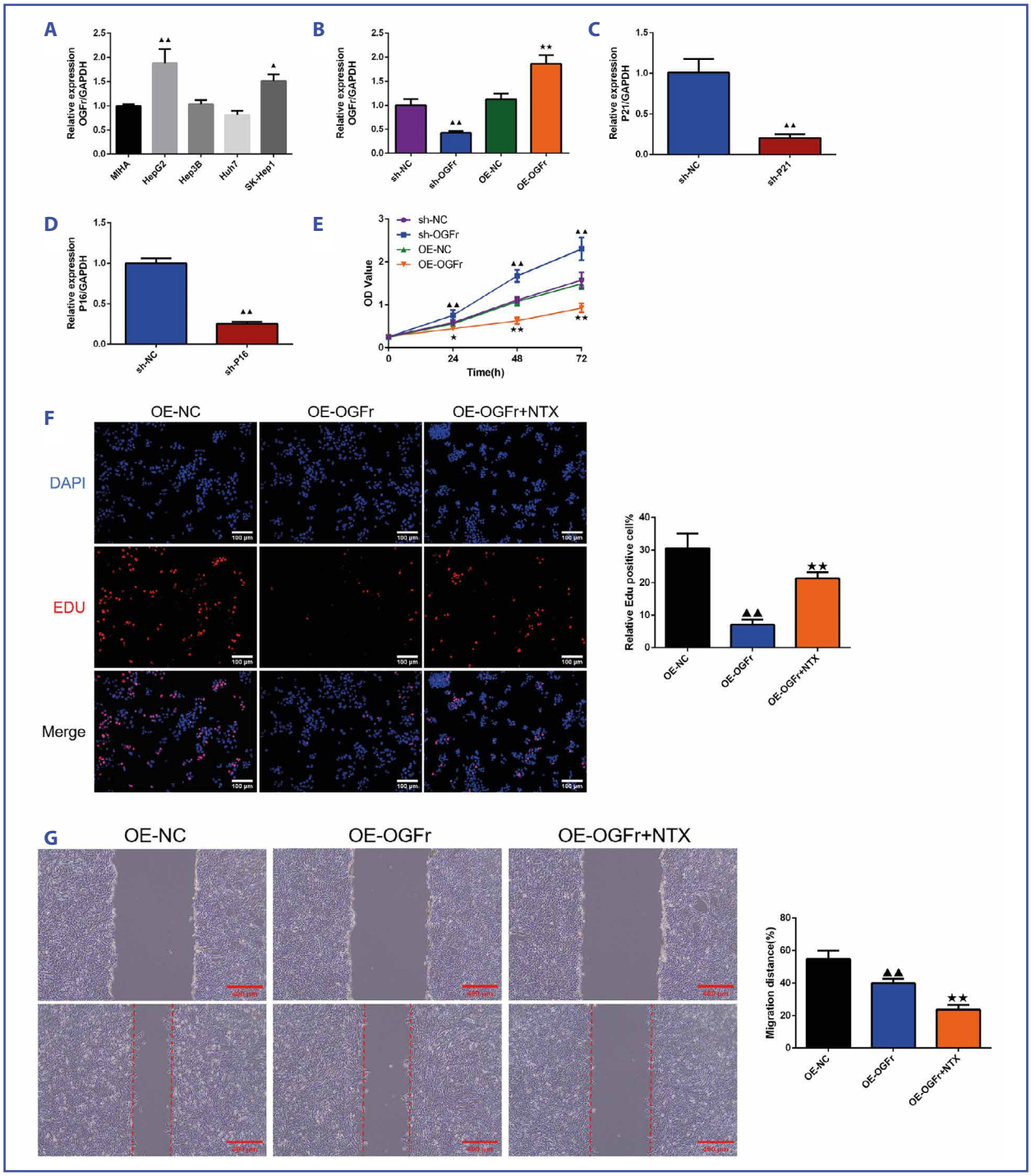

Figure 3. OGFr overexpression inhibited HepG2 cell viability, cell proliferation and migration; **A.** OGFr mRNA expression in MIHA, HepG2, Huh7, Hep3B, and SK-Hep1 cells was measured by qRT-PCR, n = 3, ▲P < 0.05 and ▲▲P < 0.01 *vs.* MIHA group. Measurements of OGFr (**B**), P21 (**C**), and P16 (**D**) mRNA levels were carried out by qRT-PCR assay for transfection efficiency validation, n = 3, ▲P < 0.05 and ▲▲P < 0.01 *vs.* sh-NC group, ★P < 0.05 and ★★P < 0.01 *vs.* OE-NC group; **E.** Cell viability at 0 h, 24 h, 48 h and 72 h was measured by CCK8 assay, n = 6, ▲P < 0.05 and ▲▲P < 0.01 *vs.* sh-NC group, ★P < 0.05 and ★★P < 0.01 *vs.* OE-NC group; **F.** Cell proliferation was assessed by EDU staining (magnification: 200×, scale bar: 100 μm), n = 3; **G**: Cell migration was determined by cell scratch assay (magnification: 40×, scale bar: 400 μm), n = 3. ▲P < 0.05 and ▲▲P < 0.01 *vs.* sh-NC group, ★P < 0.05 and ★★P < 0.01 *vs.* sh-OGFr group. Abbreviations: EDU — 5-ethynyl-2′-deoxyuridine; NTX — naltrexone; OGFr — opioid growth factor receptor.

expression occurred in HepG2 and SK-Hep1 cells compared to that of MIHA cells ($P < 0.01$ or $P < 0.05$). Therefore, HepG2 cells were selected for subsequent studies. The measurement of OGFr, P21, and P16 mRNA levels was carried out by qRT-PCR assay for transfection efficiency validation (Fig. 3B–D). The HepG2 cells in the sh-OGFr group showed lower OGFr mRNA expression than in the sh-NC group ($P < 0.01$), and there were higher OGFr mRNA levels in the OE-OGFr group than in the OE-NC group ($P < 0.01$). There were decreased P21 mRNA levels in the sh-P21 group than in the sh-NC group ($P < 0.01$), and lower P16 mRNA expression in the sh-P16 group than in the sh-NC group ($P < 0.01$). Subsequently, the determination of cell viability at 0 h, 24 h, 48 h and 72 h was done by CCK8 assay (Fig. 3E). It was evident that HepG2 cells of the sh-OGFr group showed a highly significant increase in cell activity at 24 h, 48 h and 72 h ($P < 0.01$). The OE-OGFr treatment caused a highly significant decrease of cell activity at 24 h, 48 h and 72 h ($P < 0.01$ or $P < 0.05$). In addition, detection of cell proliferation and cell migration in the OE-NC, OE-OGFr, and OE-OGFr+NTX groups was performed by EDU staining and cell scratch assay (Fig. 3F, G). The OE-OGFr group caused highly significantly reduced EDU-staining positive cells, as proliferation rate, compared to the OE-NC group (Fig. 3F, $P < 0.01$). Further NTX intervention in the OE-OGFr group led to very significantly higher EDU-staining positive cells ($P < 0.01$). In Fig. 3G, HepG2 cells in the OE-OGFr group exhibited a highly significant decrease of cell migration ability compared to that in the OE-NC group ($P < 0.01$). There was a highly significant greater reduction of cell migration ability in the OE-OGFr+NTX group than in the OE-OGFr group ($P < 0.01$).

OGFr knockdown inhibited HepG2 cell proliferation and migration by promoting P21 and P16 expression

The measurement of cell proliferation was carried out with EDU staining (Fig. 4A). The HepG2 cells in the sh-OGFr group had highly significant increases of EDU-staining positive cells compared to the sh-NC group ($P < 0.01$). We also found that sh-OGFr+sh-P21 and sh-OGFr+sh-P16 intervention led to more highly enhanced EDU-staining positive cells than in the sh-OGFr group ($P < 0.01$). Furthermore, a cell migration test was made by cell scratch assay (Fig. 4B). There was more enhanced cell migration ability in HepG2 cells of the sh-OGFr group than in the sh-NC group ($P < 0.05$). Following further sh-P21 and sh-P16 treatment respectively, OGFr knockdown increased cell migration ability in HepG2 cells ($P < 0.01$ or $P < 0.05$). Western blot assay was employed to examine P21, P16, and P53 protein expression in HepG2 cells (Fig. 4C). The OGFr knockdown treatment caused lower P21, P16, and P53 protein expression than in cells in the sh-NC group ($P < 0.01$ or $P < 0.05$). There was reduced P21 and P53 protein expression in the sh-OGFr+sh-P21 group ($P < 0.01$), as well as lower P16 and P53 protein levels in the sh-OGFr+sh-P16 group than in the sh-OGFr group ($P < 0.01$).

DISCUSSION

Hepatocellular carcinoma represents the sixth most common type of cancer and is the second leading cause of cancer death [19]. The morbidity and mortality rates of HCC continue to increase meanwhile, and it has been reported that its 5-year survival rate is only 18%, thus seriously jeopardising worldwide health and quality of life [20]. Surgical resection and liver transplantation are primarily employed in the early stages of HCC [21]. Immunosuppressive and targeted therapies are integral parts of advanced HCC treatment, although these strategies ultimately contribute to the development of drug resistance or relapse [21]. Therefore, the present study was aimed at finding potential therapeutic targets and mechanisms for HCC.

It has been demonstrated that OGF presents one of the new potential options for safe cancer treatment, accompanied by anti-tumour, analgesic, and immune-enhancing properties [22]. HCC tissues have demonstrated lower OGFr expression than adjacent normal liver tissues [23]. Wu *et al.* [23] applied transcriptomic and quantitative proteomic analyses to reveal that the long-stranded noncoding RNA HOX transcriptional antisense RNA contributed to HCC cell proliferation with negative regulation of OGFr. OGFr knockdown promoted HCC cell proliferation and G1/S phase, whereas OGFr overexpression was shown to induce inhibition of cell proliferation and G1-phase arrest [23], which is consistent with our CCK8 and EDU staining results. At the same time, NTX intervention, the OGFr antagonist in our study, reversed the antiproliferative effects of OGFr overexpression. In addition, long-stranded noncoding RNA LINC00673 has been shown to contribute to cell proliferation, migration, and invasion in epithelial ovarian cancer mediated by OGFr inhibition [24], an observation in strong agreement with the findings of our study. Notably, it has been revealed that low-dose NTX (LDN) has potentially therapeutic benefits for several cancers, including breast cancer, liver cancer, lung cancer, and colon cancer [25]. The use of LDN as an adjuvant therapy for cancer chemotherapy and immunotherapy is supported by its unique mechanism of action on cancer cells, lack of cytotoxicity, and immunomodulatory function [26]. At the same time, NTX inhibits chemotherapy-induced cardiotoxicity and thus exerts cardiomyoprotective effects, which has the potential to improve cardiac function in cancer patients [27].

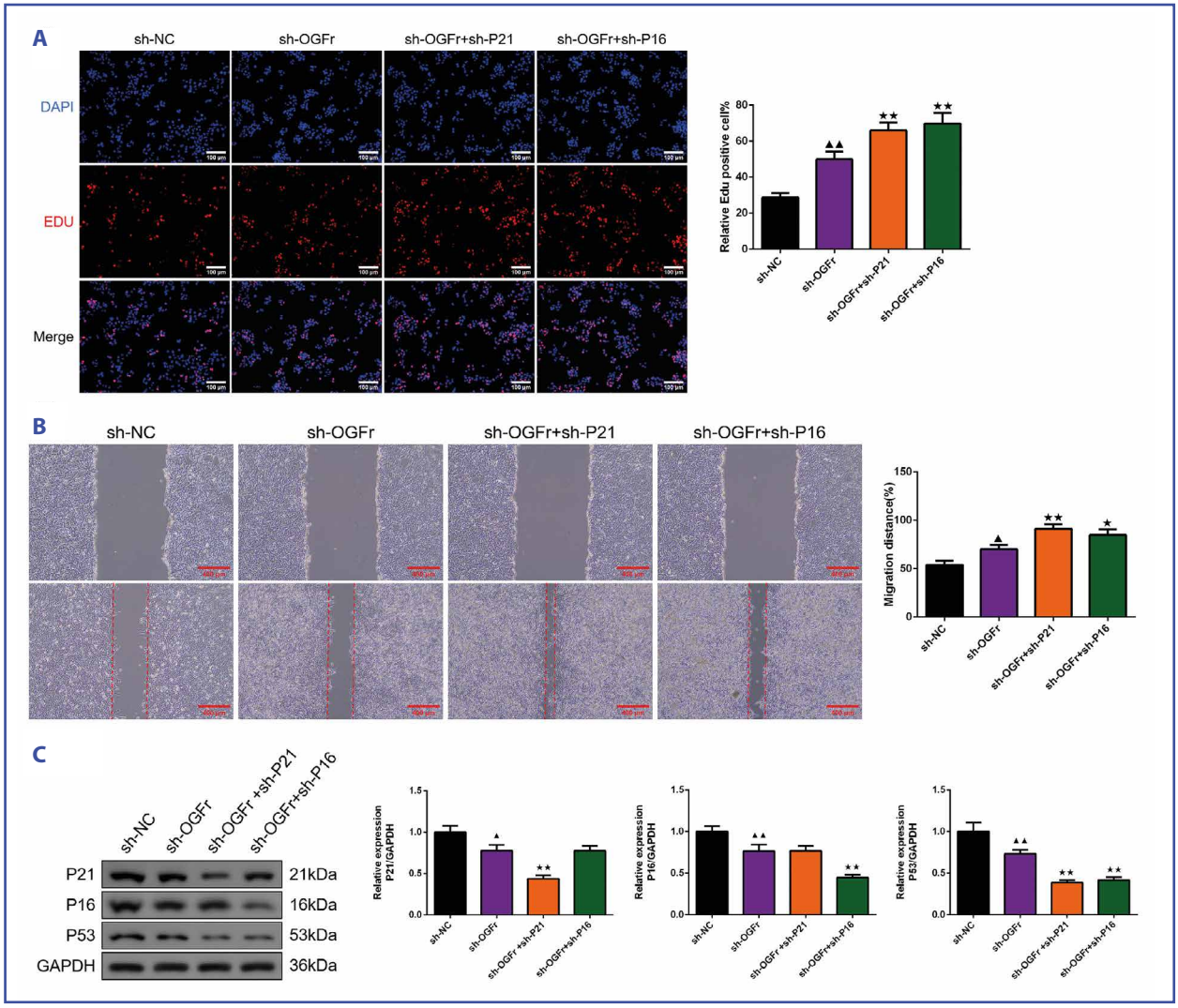

Figure 4. OGFr knockdown inhibited HepG2 cell proliferation and migration by promoting P21 and P16 expression; **A.** Measurement of cell proliferation was carried out with EDU staining (magnification: 200×, scale bar: 100 μm), n = 3; **B.** Cell migration test was made by cell scratch assay (magnification: 40×, scale bar: 400 μm), n = 3; **C.** Western blot assay was employed to examine P21, P16, and P53 protein expression in HepG2 cells, n = 3. $^{\blacktriangle}P < 0.05$ and $^{\blacktriangle\blacktriangle}P < 0.01$ *vs.* sh-NC group, $^{\star}P < 0.05$ and $^{\star\star}P < 0.01$ *vs.* sh-OGFr group. Abbreviations: EDU — 5-ethynyl-2′-deoxyuridine; OGFr — opioid growth factor receptor.

These findings may be the reasons why NTX further enhances the inhibitory effect of OGFr overexpression on cell migration in the present study. Moreover, the OGF-OGFr pathway exerts important regulatory roles in pancreatic carcinogenesis and progression, and exogenous OGF or OGFr upregulation has inhibited tumour growth in human pancreatic cancer cells and in nude mice [28]. In our study, overexpression of OGFr caused reduced tumour growth, including lower tumour volume and weight, as well as lower Ki67 expression. According to the above findings, overexpression of OGFr has the potential to alleviate the progression of HCC by inhibiting cell proliferation and cell migration.

OGF-OGFr restricts cell proliferation in human pancreatic cancer through the P21 pathway, whereas P21 knockdown reverses the inhibitory effects of OGF on cell proliferation [29]. The LMNA gene knockdown intervention in HepG2 cells causes reduced tumourigenicity, whereas P16 expression increases [30]. Exogenous OGF administration was shown to attenuate tumour volume growth in HCC mice, and further OGF combined with cisplatin intervention was observed to express higher OGFr, P16, P21, and P53 than the cisplatin–only intervention group, although the findings were evaluated only by immunohistochemistry [12].

In the present study, OGFr knockdown and overexpression was further carried out in HCC mice, respectively, preliminarily confirming that OGFr may exert anti-HCC effects by P16 and P21 activation. Klocek *et al.* [31] indicated that the mechanism of OGF-OGFr was independent of apoptosis in Tenon's capsule fibroblasts, and that knockdown of P16 or P21 eliminated the growth inhibitory effects of OGF

treatment. Moreover, knockdown of OGFr led to the reduction of P21 and P53 expression [12].

The above findings accord with our results. Furthermore, in ovarian cancer cells, knockdown of OGFr results in upregulated cell proliferation, and knockdown of P16 or P21 reverses the inhibitory effect of OGF on tumour growth [32]. In fact, LDN has demonstrated high anticancer potential [26]. Liu *et al.* [33] showed that LDN inhibited migration and invasion of cervical cancer cells. *In vitro*, consistent with the above findings, NTX enhanced the anti-migratory effects of OGFr overexpression in this study, and knockdown of OGFr and P16 or P21 led to enhanced cell proliferation and migration of HepG2 cells. Hence, P16 and P21 present important targets of OGFr in HCC.

The study by Avella *et al.* [13] documented the presence of OGFr in HCC cells and surgical specimens, and the ability of OGFr to inhibit the growth of HCC cells, which was related to the inhibition of DNA synthesis and was not related to apoptosis or necrosis pathways, laying a solid theoretical foundation for our present study. Sikong *et al.* [12] found that OGF inhibited migration and proliferation of HCC cells, and exogenous OGF enhanced the antitumour activity of cisplatin on HCC by upregulating P21 and P53. The present study mainly focused on the role and potential mechanism of OGFr action in HCC, which may inhibit cell proliferation and migration by activating P16 and P21 thus exerting anti-tumour activity, and it preliminarily confirmed that these actions were not related to apoptosis.

However, interestingly, OGF and gemcitabine conjugate induced apoptosis in human pancreatic cancer cell line MIA PaCa-2 cells, whereas apoptosis was not detected in human metastatic pancreatic tumour cell line AsPC-1 cells [9]. Additionally, in cutaneous squamous cell carcinoma, OGFr led to G0/G1 cell cycle arrest and activation of apoptosis [34]. Therefore, subsequent investigations are required to gain a deeper understanding of the mechanism of OGFr action in various tumour types.

CONCLUSIONS

With the establishment of an HCC tumour model in nude mice and the application of HepG2 cells, we have verified both *in vitro* and *in vivo* that OGFr may exert anti-HCC effects by activating P16 and P21, and thus inhibit HCC cell proliferation and migration. These findings may contribute to the development of new strategies and potential targets for HCC treatment.

Article information and declarations

Data availability statement

The datasets used and/or analysed during the current study are available from the corresponding author upon reasonable request.

Ethics statement

All animal experiments in this work were granted by the Animal Experimentation Ethics Committee of Hangzhou Huante Youjian Biotechnology Centre (Certificate No. SYXK (Zhe) 2024-0003) and conducted following the guidelines of the Institutional Animal Care and Use Committee (approval number: ZJEY-20240215-01).

Authors' contributions

ZJ, YJ: collected and analysed data; ZJ: conceptualised this research, major contributor to writing manuscript; YJ: revised paper. Both authors read and approved the final manuscript.

Funding

This work was supported by Zhejiang Provincial Medical and Health Science and Technology Plan (grant number 2020KY736).

Conflicts of interest

The authors have no competing interests to declare that are relevant to the content of this article.

Supplementary materials

Supplementary Material is available on Journal's website. This includes:

Supplementary Table S1. Raw data of tumour volumes.
Supplementary Table S2. Raw data of tumour weights.
Supplementary Table S3. Raw data of tumour inhibition rates.

REFERENCES

1. Llovet JM, Kelley RK, Villanueva A, et al. Hepatocellular carcinoma. Nat Rev Dis Primers. 2021; 7(1): 6, doi: 10.1038/s41572-020-00240-3, indexed in Pubmed: 33479224.
2. Chidambaranathan-Reghupaty S, Fisher PB, Sarkar D. Hepatocellular carcinoma (HCC): Epidemiology, etiology and molecular classification. Adv Cancer Res. 2021; 149: 1–61, doi: 10.1016/bs.acr.2020.10.001, indexed in Pubmed: 33579421.
3. Wang Yu, Deng B. Hepatocellular carcinoma: molecular mechanism, targeted therapy, and biomarkers. Cancer Metastasis Rev. 2023; 42(3): 629–652, doi: 10.1007/s10555-023-10084-4, indexed in Pubmed: 36729264.
4. Yang C, Zhang H, Zhang L, et al. Evolving therapeutic landscape of advanced hepatocellular carcinoma. Nat Rev Gastroenterol Hepatol. 2023; 20(4): 203–222, doi: 10.1038/s41575-022-00704-9, indexed in Pubmed: 36369487.
5. Rimassa L, Wörns MA. Navigating the new landscape of second-line treatment in advanced hepatocellular carcinoma. Liver Int. 2020; 40(8): 1800–1811, doi: 10.1111/liv.14533, indexed in Pubmed: 32432830.
6. Wang R, Zhang Yi, Shan F. Interaction of opioid growth factor (OGF) and opioid antagonist and their significance in cancer therapy. Int Immunopharmacol. 2019; 75: 105785, doi: 10.1016/j.intimp.2019.105785, indexed in Pubmed: 31404891.
7. Huang H, Liu B, Qu Na, et al. Research progress of opioid growth factor in immune-related diseases and cancer diseases. Int Immunopharmacol. 2021; 99: 107713, doi: 10.1016/j.intimp.2021.107713, indexed in Pubmed: 34426103.
8. Qu Na, Wang X, Meng Y, et al. Prospective oncotarget for gynecological cancer: Opioid growth factor (OGF) — opioid growth factor receptor (OGFr) axis. Int Immunopharmacol. 2019; 75: 105723, doi: 10.1016/j.intimp.2019.105723, indexed in Pubmed: 31408839.
9. Budka J, Debowski D, Mai S, et al. Design, synthesis, and antitumor evaluation of an opioid growth factor bioconjugate targeting pancreatic ductal adenocarcinoma. Pharmaceutics. 2024; 16(2), doi: 10.3390/pharmaceutics16020283, indexed in Pubmed: 38399336.

10. McLaughlin PJ, Verderame MF, Hankins JL, et al. Overexpression of the opioid growth factor receptor downregulates cell proliferation of human squamous carcinoma cells of the head and neck. Int J Mol Med. 2007; 19(3): 421–428, indexed in Pubmed: 17273790.
11. Huang H, Wang X, Zhang S, et al. *In vitro* and *in vivo* killing effects of methionine enkephalin on osteosarcoma. Int Immunopharmacol. 2023; 125(Pt B): 111226, doi: 10.1016/j.intimp.2023.111226, indexed in Pubmed: 37976597.
12. Sikong Y, Wang Q, Cai M, et al. Exogenous OGF enhances the anti-tumor activity of cisplatin on hepatocellular carcinoma. Int J Clin Exp Pathol. 2019; 12(2): 590–598, indexed in Pubmed: 31933864.
13. Avella DM, Kimchi ET, Donahue RN, et al. The opioid growth factor-opioid growth factor receptor axis regulates cell proliferation of human hepatocellular cancer. Am J Physiol Regul Integr Comp Physiol. 2010; 298(2): R459–R466, doi: 10.1152/ajpregu.00646.2009, indexed in Pubmed: 19923357.
14. Cheng F, McLaughlin PJ, Verderame MF, et al. The OGF-OGFr axis utilizes the p16INK4a and p21WAF1/CIP1 pathways to restrict normal cell proliferation. Mol Biol Cell. 2009; 20(1): 319–327, doi: 10.1091/mbc.e08-07-0681, indexed in Pubmed: 18923142.
15. Cheng F, Zagon IS, Verderame MF, et al. The opioid growth factor (OGF)-OGF receptor axis uses the p16 pathway to inhibit head and neck cancer. Cancer Res. 2007; 67(21): 10511–10518, doi: 10.1158/0008-5472.CAN-07-1922, indexed in Pubmed: 17974995.
16. Xiang Z, Miao Q, Zhang J, et al. AB4 inhibits Notch signaling and promotes cancer cell apoptosis in liver cancer. Oncol Rep. 2021; 45(6), doi: 10.3892/or.2021.8063, indexed in Pubmed: 33907837.
17. Wang P, Sun J, Sun C, et al. BTF3 promotes proliferation and glycolysis in hepatocellular carcinoma by regulating GLUT1. Cancer Biol Ther. 2023; 24(1): 2225884, doi: 10.1080/15384047.2023.2225884, indexed in Pubmed: 37382415.
18. Kučić N, Rački V, Šverko R, et al. Immunometabolic modulatory role of naltrexone in BV-2 microglia cells. Int J Mol Sci. 2021; 22(16), doi: 10.3390/ijms22168429, indexed in Pubmed: 34445130.
19. Shah M, Sarkar D. HCC-related lncRNAs: roles and mechanisms. Int J Mol Sci. 2024; 25(1), doi: 10.3390/ijms25010597, indexed in Pubmed: 38203767.
20. Hao X, Sun G, Zhang Y, et al. Targeting immune cells in the tumor microenvironment of HCC: new opportunities and challenges. Front Cell Dev Biol. 2021; 9: 775462, doi: 10.3389/fcell.2021.775462, indexed in Pubmed: 34869376.
21. Chakraborty E, Sarkar D. Emerging therapies for hepatocellular carcinoma (HCC). Cancers (Basel). 2022; 14(11), doi: 10.3390/cancers14112798, indexed in Pubmed: 35681776.
22. Budka J, Kowalski S, Chylinska M, et al. Opioid growth factor and its derivatives as potential non-toxic multifunctional anticancer and analgesic compounds. Curr Med Chem. 2021; 28(4): 673–686, doi: 10.2174/0929867327666200304122406, indexed in Pubmed: 32129162.
23. Wu Y, Xiong Q, Li S, et al. Integrated proteomic and transcriptomic analysis reveals long noncoding RNA HOX transcript antisense intergenic RNA (HOTAIR) promotes hepatocellular carcinoma cell proliferation by regulating opioid growth factor receptor (ogfr). Mol Cell Proteomics. 2018; 17(1): 146–159, doi: 10.1074/mcp.RA117.000277, indexed in Pubmed: 29079719.
24. Zheng T, Qiu J, Li C, et al. Long noncoding RNA LINC00673 promotes the proliferation and metastasis of epithelial ovarian cancer by associating with opioid growth factor receptor. Onco Targets Ther. 2019; 12: 6145–6156, doi: 10.2147/OTT.S209784, indexed in Pubmed: 31496722.
25. Couto RD, Fernandes BJ. Low doses naltrexone: the potential benefit effects for its use in patients with cancer. Curr Drug Res Rev. 2021; 13(2): 86–89, doi: 10.2174/2589977513666210127094222, indexed in Pubmed: 33504322.
26. Ciwun M, Tankiewicz-Kwedlo A, Pawlak D. Low-dose naltrexone as an adjuvant in combined anticancer therapy. Cancers (Basel). 2024; 16(6), doi: 10.3390/cancers16061240, indexed in Pubmed: 38539570.
27. Liu C, Cheng X, Xing J, et al. CIRBP-OGFR axis safeguards against cardiomyocyte apoptosis and cardiotoxicity induced by chemotherapy. Int J Biol Sci. 2022; 18(7): 2882–2897, doi: 10.7150/ijbs.69655, indexed in Pubmed: 35541895.
28. Zagon IS, McLaughlin PJ. Opioid growth factor and the treatment of human pancreatic cancer: a review. World J Gastroenterol. 2014; 20(9): 2218–2223, doi: 10.3748/wjg.v20.i9.2218, indexed in Pubmed: 24605021.
29. Cheng F, McLaughlin PJ, Verderame MF, et al. The OGF-OGFr axis utilizes the p21 pathway to restrict progression of human pancreatic cancer. Mol Cancer. 2008; 7: 5, doi: 10.1186/1476-4598-7-5, indexed in Pubmed: 18190706.
30. Liu H, Li D, Zhou L, et al. LMNA functions as an oncogene in hepatocellular carcinoma by regulating the proliferation and migration ability. J Cell Mol Med. 2020; 24(20): 12008–12019, doi: 10.1111/jcmm.15829, indexed in Pubmed: 32896989.
31. Klocek MS, Sassani JW, Donahue RN, et al. Regulation of Tenon's capsule fibroblast cell proliferation by the opioid growth factor and the opioid growth factor receptor axis. Invest Ophthalmol Vis Sci. 2010; 51(10): 5054–5061, doi: 10.1167/iovs.09-4949, indexed in Pubmed: 20463323.
32. Donahue RN, McLaughlin PJ, Zagon IS. Cell proliferation of human ovarian cancer is regulated by the opioid growth factor-opioid growth factor receptor axis. Am J Physiol Regul Integr Comp Physiol. 2009; 296(6): R1716–R1725, doi: 10.1152/ajpregu.00075.2009, indexed in Pubmed: 19297547.
33. Liu N, Yan L, Shan F, et al. Low-dose naltrexone plays antineoplastic role in cervical cancer progression through suppressing PI3K/AKT/mTOR pathway. Transl Oncol. 2021; 14(4): 101028, doi: 10.1016/j.tranon.2021.101028, indexed in Pubmed: 33540155.
34. Bai X, Shan F, Qu Na, et al. Regulatory role of methionine enkephalin in myeloid-derived suppressor cells and macrophages in human cutaneous squamous cell carcinoma. Int Immunopharmacol. 2021; 99: 107996, doi: 10.1016/j.intimp.2021.107996, indexed in Pubmed: 34311187.